Higher order hierarchical discretization scheme for surface integral equations for layered media

Jørgensen, Erik; Kim, Oleksiy S.; Meincke, Peter; Breinbjerg, Olav

Published in:
I E E E Transactions on Geoscience and Remote Sensing

Link to article, DOI:
10.1109/TGRS.2003.819881

Publication date:
2004

Document Version
Publisher's PDF, also known as Version of record

Higher Order Hierarchical Discretization Scheme for Surface Integral Equations for Layered Media

Erik Jørgensen, *Member, IEEE*, Oleksiy S. Kim, Peter Meincke, *Member, IEEE*, and Olav Breinbjerg, *Member, IEEE*

***Abstract*—This paper presents an efficient technique for the analysis of electromagnetic scattering by arbitrarily shaped perfectly conducting objects in layered media. The technique is based on a higher order method of moments (MoM) solution of the electric field, magnetic field, or combined-field integral equation. This higher order MoM solution comprises higher order curved patches for the geometry modeling and higher order hierarchical basis functions for expansion of the electric surface current density. Due to the hierarchical property of the basis functions, the order of the expansion can be selected separately on each patch depending on the wavelength in the layer in which the patch is located and the size of the patch. In this way, a significant reduction of the number of unknowns is achieved and the same surface mesh can be reused in a wide frequency band. It is shown that even for fairly large problems, the higher order hierarchical MoM requires less memory than existing fast multipole method (FMM) or multilevel FMM implementations.**

***Index Terms*—Combined-field integral equation (CFIE), electromagnetic scattering, higher order hierarchical vector basis functions, layered media, Legendre polynomial, method of moments (MoM), perfectly conducting (PEC) object.**

I. Introduction

THE SURFACE integral equation method is a well-known and elaborated technique for the analysis of scattering by perfectly conducting (PEC) objects. When solving this integral equation by the method of moments (MoM), the selection of basis functions is a crucial point. Traditionally, the Rao–Wilton–Glisson (RWG) [1] or rooftop basis functions [2], known from free-space configurations, are also employed in multilayered environments [3]–[5]. The piecewise linear expansion of the current utilized in these low-order methods requires a mesh with the patch size based on the wavelength in the surrounding medium, such that the patch size decreases as the permittivity of the medium increases. Moreover, for objects penetrating the interface between layers, the low-order methods cannot efficiently handle the different wavelengths in different media. Consequently, a uniform mesh based on the shortest wavelength is used, but this introduces unnecessary unknowns for the part of the object that is located in the media with low permittivity, leading to a poor condition number of the resulting MoM matrix. Alternatively, low-order methods may employ a nonuniform mesh at the interface between media. This kind of mesh can be difficult to construct, especially if the difference in permittivity is large, and this nonuniform mesh may result in ill-conditioning.

The application of higher order basis functions is one of the ways to relax computational demands when large-scale electromagnetic problems are solved in free space. The discretization with higher order basis functions allows the number of unknowns to be reduced, while the accuracy of the solution is retained. Another advantage of higher order basis functions is that the meshing of the object can be done once and then reused in a wide frequency band with variable order of the basis functions. The higher order approach is also very promising for problems involving layered media. For such media, the computation of the Green's functions is relatively time consuming, and therefore, reducing the number of unknowns is of great importance. Furthermore, the overall number of integration points in which the Green's function needs to be calculated also reduces, since each point can be reused for a large number of the higher order functions defined on the same patch. Nevertheless, there are only few papers dedicated to higher order bases in multilayered media. Interpolatory basis functions were applied in [6] for electromagnetic analysis of multilayer microstrip antennas. Although interpolatory bases work well for microstrip problems, they can cause the same mesh problem as low-order methods when the object spans two or more media, since the current expansion order is fixed for the whole geometry. Popović *et al.* [7] employed higher order hierarchical power basis functions for solving a thin-wire antenna problem near, or in, a lossy ground. Hierarchical basis functions were used for simulation of conducting surfaces in layered media in [8], but results were not presented for expansion orders higher than two. Also, the basis functions were not orthogonal, which required the use of an inefficient direct matrix solver due to ill-conditioning of the resulting MoM matrix. Moreover, the order of the basis function along the direction of the current and along the transverse direction were fixed to be the same, making them incompatible with the Nedelec constraint [9] and requiring patches with nearly equal side length. Also, it seems that the polynomial expansion order was not selected according to the wavelength in different media, and, consequently, the advantage of the hierarchical basis functions was not fully exploited.

In this paper, we utilize higher order hierarchical vector basis functions, recently developed for free space [10], for the electromagnetic analysis of PEC objects in layered media. Hierarchical basis functions are more advantageous than interpolatory functions, since the current expansion order can be selected separately for each patch. Moreover, for multilayered media,

Manuscript received January 24, 2003; revised September 3, 2003. This work was supported by the Danish Technical Research Council.

E. Jørgensen was with Ørsted-DTU, Section for Electromagnetic Systems, Technical University of Denmark, Lyngby, Denmark. He is now with TICRA, DK-1201 Copenhagen, Denmark (e-mail: ej@ticra.com).

O. S. Kim, P. Meincke, and O. Breinbjerg are with Ørsted-DTU, Section for Electromagnetic Systems, Technical University of Denmark, Lyngby, Denmark (e-mail: osk@oersted.dtu.dk; pme@oersted.dtu.dk; ob@oersted.dtu.dk).

Digital Object Identifier 10.1109/TGRS.2003.819881

the expansion order can be selected adaptively, depending on the wavelength in the layer in which the patch is located. The basis functions used here automatically satisfy continuity of the normal component of the surface current flowing between adjacent patches, and the lowest order expansion is the well-known rooftop function. Independent selection of the expansion order along the direction of the current and along the transverse direction makes the discretization technique flexible and compatible with the Nedelec constraint. Furthermore, the expansion of the surface current density is nearly orthogonal, whereas the surface charge density is implicitly expanded in orthogonal functions. This property allows the condition number of the MoM matrix to be reduced by several orders of magnitudes in comparison with higher order hierarchical basis functions derived without considering the orthogonality of the basis functions [8], [11]. Due to this improvement, an iterative matrix solver can be employed even for high expansion orders. The basis functions are defined on higher order curvilinear quadrilateral patches that provide accurate representation of the geometry using rather large patches.

Throughout the paper, we deal with the combined-field integral equation (CFIE), so that the results are applicable for both the electric field (EFIE) and magnetic field (MFIE) integral equations. The problem of applying MFIE for scattering by PEC objects in layered media was addressed in [12], but only for the special case of bodies of revolution (MFIE–BOR method). Here, we consider a general problem of arbitrary closed PEC objects in layered media.

The paper is organized as follows. Section II contains the description of the higher order hierarchical MoM scheme. In Section III, the higher order convergence of the method is proved by comparing with analytical results for a PEC sphere in free space. Numerical results for a half-buried PEC sphere and an unexploded ordnance (UXO) illuminated by a plane wave are also given in Section III. In this section, the computational complexity and memory requirements of the presented method are discussed and compared with existing fast multipole method (FMM) and multilevel fast multipole method (MLFMM) implementations. In Section IV, some concluding remarks are made.

The time factor $e^{j\omega t}$ is assumed and suppressed throughout the paper.

II. Higher Order Hierarchical MoM

A. Integral Equation for Layered Medium

For a closed PEC object the CFIE takes on the following form:

$$\begin{aligned}\alpha\hat{\mathbf{n}}\times\mathbf{E}^{\mathrm{inc}}(\mathbf{r})+(1-\alpha)\eta(\mathbf{r})\hat{\mathbf{n}}\times\mathbf{H}^{\mathrm{inc}}(\mathbf{r})\\ =-\alpha\hat{\mathbf{n}}\times\mathbf{E}^{\mathrm{scat}}(\mathbf{r})+(1-\alpha)\eta(\mathbf{r})\mathbf{J}_s(\mathbf{r})\\ -(1-\alpha)\eta(\mathbf{r})\hat{\mathbf{n}}\times\mathbf{H}^{\mathrm{scat}}(\mathbf{r}),\qquad \mathbf{r}\in S.\end{aligned}\tag{1}$$

Herein $\mathbf{E}^{\mathrm{inc}}(\mathbf{r})$ and $\mathbf{H}^{\mathrm{inc}}(\mathbf{r})$ are the incident electric and magnetic fields, α is a real number between 0 and 1, $\mathbf{r}$ denotes the observation point, $\eta(\mathbf{r})$ is the intrinsic impedance of the medium at the observation point, and $\hat{\mathbf{n}}$ is an outward normal unit vector to the surface of the object S. For the open parts of the object, α is set to 1, reducing (1) to the EFIE.

The scattered electric field due to the surface current density $\mathbf{J}_s(\mathbf{r})$ and the surface charge density $\rho_s(\mathbf{r})$ can be expressed in a mixed-potential form as

$$\begin{aligned}\mathbf{E}^{\mathrm{scat}}(\mathbf{r})=-j\omega\int_S\bar{\mathbf{K}}_A^{\mathrm{EFIE}}(\mathbf{r},\mathbf{r}')\cdot\mathbf{J}_s(\mathbf{r}')\,dS'\\ -\nabla\int_S K_\phi(\mathbf{r},\mathbf{r}')\rho_s(\mathbf{r}')dS',\qquad \mathbf{r}\in S\end{aligned}\tag{2}$$

where $\bar{\mathbf{K}}_A^{\mathrm{EFIE}}(\mathbf{r},\mathbf{r}')$ is the EFIE dyadic kernel and $K_\phi(\mathbf{r},\mathbf{r}')$ is the EFIE scalar kernel. These functions are derived using formulation C by Michalski and Zheng [4]. $\mathbf{J}_s(\mathbf{r})$ and $\rho_s(\mathbf{r})$ satisfy the equation of continuity

$$\nabla_s\cdot\mathbf{J}_s(\mathbf{r})=-j\omega\rho_s(\mathbf{r}).\tag{3}$$

The scattered magnetic field on S is given by

$$\begin{aligned}\hat{\mathbf{n}}\times\mathbf{H}^{\mathrm{scat}}(\mathbf{r})&=\hat{\mathbf{n}}\times\nabla\times\int_S\bar{\mathbf{G}}_A(\mathbf{r},\mathbf{r}')\cdot\mathbf{J}_s(\mathbf{r}')\,dS'\\ &=\frac{\Omega}{4\pi}\mathbf{J}_s(\mathbf{r})+\hat{\mathbf{n}}\times\fint_S[\nabla\times\bar{\mathbf{G}}_A(\mathbf{r},\mathbf{r}')]\\ &\quad\cdot\mathbf{J}_s(\mathbf{r}')\,dS',\qquad \mathbf{r}\in S\end{aligned}\tag{4}$$

where Ω is the solid angle subtended by the surface at the point $\mathbf{r}$ [13], $\fint_S$ denotes the principal value integral over S, and $\bar{\mathbf{G}}_A$ is the dyadic Green's function for the magnetic vector potential in layered media in its traditional form [14]

$$\bar{\mathbf{G}}_A=(\hat{\mathbf{x}}\hat{\mathbf{x}}+\hat{\mathbf{y}}\hat{\mathbf{y}})G_{xx}+\hat{\mathbf{z}}\hat{\mathbf{x}}G_{zx}+\hat{\mathbf{z}}\hat{\mathbf{y}}G_{zy}+\hat{\mathbf{z}}\hat{\mathbf{z}}G_{zz}.\tag{5}$$

Thus, we can define the MFIE dyadic kernel $\bar{\mathbf{K}}_A^{\mathrm{MFIE}}(\mathbf{r},\mathbf{r}')$ as

$$\begin{aligned}\bar{\mathbf{K}}_A^{\mathrm{MFIE}}(\mathbf{r},\mathbf{r}')&=\nabla\times\bar{\mathbf{G}}_A(\mathbf{r},\mathbf{r}')\\ &=\begin{bmatrix}\frac{\partial G_{xx}}{\partial y} & \frac{\partial G_{zy}}{\partial y}-\frac{\partial G_{xx}}{\partial z} & \frac{\partial G_{zz}}{\partial y}\\ \frac{\partial G_{xx}}{\partial z}-\frac{\partial G_{zx}}{\partial x} & -\frac{\partial G_{zy}}{\partial x} & -\frac{\partial G_{zz}}{\partial x}\\ -\frac{\partial G_{xx}}{\partial y} & \frac{\partial G_{xx}}{\partial x} & 0\end{bmatrix}.\end{aligned}\tag{6}$$

The expressions for the elements of the dyadics $\bar{\mathbf{G}}_A(\mathbf{r},\mathbf{r}')$, and $\bar{\mathbf{K}}_A^{\mathrm{EFIE}}(\mathbf{r},\mathbf{r}')$ as well as for $K_\phi(\mathbf{r},\mathbf{r}')$ can be derived in closed form in the spectral domain [4], [15]. In the spatial domain, we need to evaluate Sommerfeld integrals of the form

$$G(\mathbf{r},\mathbf{r}')=\frac{1}{4\pi}\int_{\mathrm{SIP}}k_\rho H_0^{(2)}(k_\rho\rho)\tilde{G}(k_\rho)dk_\rho\tag{7}$$

where SIP denotes the Sommerfeld integration path, $\tilde{G}$ is the spectral domain counterpart of G, and $H_0^{(2)}$ is the zeroth-order Hankel function of the second kind. Numerical integration of these improper integrals is very time consuming, even if the integration is performed along the steepest descent path [16]. Therefore, the more efficient discrete complex image method (DCIM) [17]–[22] is employed in this paper. This method, which is briefly revisited in the next section, allows the spatial Green's functions to be represented in closed form in terms of complex images.

B. Complex-Image Representation of the Green's Functions

First, the direct field $\tilde{G}^0$ and surface-wave contributions $\tilde{G}^{\rm sw}$ are extracted from $\tilde{G}$ [17], [21]

$$\tilde{G}(k_\rho) = \tilde{G}^0(k_\rho) + \tilde{G}^{\rm sw}(k_\rho) + \tilde{G}^r(k_\rho). \tag{8}$$

Then, the remaining part $\tilde{G}^r$ of $\tilde{G}$ is expanded in a series of complex exponential functions using the generalized pencil-of-function method [23]

$$\tilde{G}^r(k_\rho) \simeq \frac{2\pi}{j}\sum_{n=1}^{N} c_n \frac{e^{-a_n k_z}}{k_z} \tag{9}$$

where c_n and a_n are known complex coefficients, and $k_z = \sqrt{k^2 - k_\rho^2}$.

Finally, via the Sommerfeld identity

$$\frac{e^{-jkr}}{r} = -\frac{j}{2}\int_{\rm SIP} \frac{k_\rho}{k_z} H_0^{(2)}(k_\rho \rho) e^{-jk_z|z|} dk_\rho \tag{10}$$

the Green's functions in the spatial domain can be obtained in closed form as

$$G^r(\mathbf{r},\mathbf{r}') \simeq \sum_{n=1}^{N} c_n \frac{e^{-jkr_n}}{r_n} \tag{11}$$

where $r_n = \sqrt{\rho^2 - a_n^2}$ is a complex distance. The corresponding elements of the dyadic $\bar{\mathbf{K}}_A^{\rm MFIE}(\mathbf{r},\mathbf{r}')$ can easily be derived from (11) and (6).

If the object is confined to one layer, G^r can be represented by several sets of complex images with coefficients that are invariant with respect to the coordinates of the source and observation points [24]. These coefficients are calculated once and stored for each dielectric layer involved in the problem, and then used in (11) to compute the Green's functions.

For objects penetrating the interface between media, the source and observation points might be located in different media and the complex image coefficients cannot be cast in the invariant form discussed above. However, a term depending on the z coordinate of either the source point or the observation point can be factored out. In our implementation, we made the complex image coefficients depend only on the z coordinate of the source point. In this way, the complex image coefficients do not need to be recalculated for each pair of source and observation points but only for different z coordinates of the source point and different observation layers. Moreover, significant savings can be obtained by computing the coefficients on a fixed grid along the z axis and use interpolation if the z coordinate of a source point does not coincide with the grid [25].

C. Discretization Scheme

The object is divided into curvilinear quadrilateral patches with local parametric coordinate systems (u,v), where $-1 \le u,v \le 1$. The polynomial degree used in the representation of the position vector $\mathbf{r}(u,v)$ defines the order of each patch; bilinear (QUAD4), quadratic (QUAD9), or orders higher than that. The surface current density $\mathbf{J}_s$ on each patch is represented as $\mathbf{J}_s(\mathbf{r}) = J_s^u(\partial\mathbf{r}/\partial u) + J_s^v(\partial\mathbf{r}/\partial v)$ where $(\partial\mathbf{r}/\partial u)$ and $(\partial\mathbf{r}/\partial v)$ are the covariant unitary vectors. The two components J_s^u and J_s^v are expanded in terms of higher order hierarchical basis functions as [10]

$$\begin{aligned} J_s^\xi = {} & \frac{\sqrt{3}}{4\mathcal{J}(\xi,\zeta)}\sum_{n=0}^{N^\zeta}[b_{0n}^\xi(1-\xi) + b_{1n}^\xi(1+\xi)]C_n^\zeta P_n(\zeta) \\ & + \frac{1}{\mathcal{J}(\xi,\zeta)}\sum_{m=2}^{M^\xi}\sum_{n=0}^{N^\zeta} b_{mn}^\xi C_m^\xi [P_m(\xi) - P_{m-2}(\xi)] C_n^\zeta P_n(\zeta) \end{aligned} \tag{12}$$

where (ξ,ζ) are (u,v) or (v,u), $\mathcal{J}(\xi,\zeta) = |(\partial\mathbf{r}/\partial\xi) \times (\partial\mathbf{r}/\partial\zeta)|$, $P_n(\xi)$ are Legendre polynomials, and b_{mn}^ξ are unknown coefficients. M^ξ and N^ζ denote the expansion order along the direction of the current and along the transverse direction, respectively. The factors $C_m^\xi = (1/2)\sqrt{((2m-3)(2m+1))/(2m-1)}$ and $C_n^\zeta = \sqrt{n+(1/2)}$ are chosen such that the Euclidean norm of each function is unity on a unit square patch. Equation (12) incorporates the necessary modifications to enforce continuity of the normal component of the surface current across patch edges while maintaining almost perfect orthogonality of the basis functions.

The charge associated with the J_s^ξ component can be obtained through the continuity equation (3) as

$$\begin{aligned} \rho_s^\xi = {} & \frac{j}{\omega}\frac{\sqrt{3}}{4\mathcal{J}(\xi,\zeta)}\sum_{n=0}^{N^\zeta}\left[-b_{0n}^\xi + b_{1n}^\xi\right] C_n^\zeta P_n(\zeta) \\ & + \frac{j}{\omega}\frac{1}{\mathcal{J}(\xi,\zeta)}\sum_{m=2}^{M^\xi}\sum_{n=0}^{N^\zeta} b_{mn}^\xi C_m^\xi (2m-1) P_{m-1}(\xi) C_n^\zeta P_n(\zeta). \end{aligned} \tag{13}$$

The higher order functions in the second line of the (13) are all mutually orthogonal and orthogonal to the low-order functions in the first line of the equation. Consequently, the current expansion in (12) implicitly yields a higher order orthogonal expansion of the surface charge density. Further details on these basis functions can be found in [10].

D. Evaluation of Self-Term Matrix Elements

When the MoM is applied to discretize the integral equation (1) using the basis functions described above, a matrix system is obtained, in which the matrix elements can be computed through a straightforward numerical quadrature scheme, e.g., Gauss–Legendre. However, an integrable singularity is present when the source and observation points are located on the same patch due to the singularity of the free-space part of the Green's function. Standard procedures, e.g., [26], for evaluating this type of integrals are based on extracting a part of the integrand that subsequently is integrated analytically. This works well with low-order basis functions but becomes extremely cumbersome as the polynomial order increases. Instead, the fully numerical annihilation procedure suggested in [27] can be applied. The original quadrilateral integration domain is divided into four new domains, each with a singularity at the origin. The Duffy transform [28] is then applied to each of the four new integration domains which leave four well-behaved integrands that can be

safely integrated using standard quadrature schemes. This singularity treatment is completely independent of the basis functions and the Green's function, which makes it ideally suited for the present application.

E. Selection of the Expansion Order

According to (12), the expansion order of the current density on each patch is defined by four parameters M^u and N^v for J_s^u, and M^v and N^u for J_s^v. Basically, these parameters can be selected independently. However, the minimum number of unknowns for a given accuracy is generally achieved by applying the Nedelec constraint [9]. This constraint imposes the condition $N^\xi = M^\xi - 1$, making the expansion complete to order N^ξ in the ξ direction. Hence, the total number of unknowns or basis functions defined on the ith patch is $N_i = (M^u + 1)M^v + (M^v + 1)M^u$. Hence, each integration point on the patch is shared by N_i basis functions and, consequently, the Green's functions computed at this point can be reused for N_i basis functions. Therefore, higher order expansions provide significant saving of computational time, especially for a layered media, where the calculation of the Green's function is a very time-consuming task. For instance, for rooftop basis functions ($M^u = M^v = 1, N^u = N^v = 0$) each integration point is shared only by $N_i = 4$ basis functions. However, for a seventh-order expansion ($M^u = M^v = 7, N^u = N^v = 6$) each integration point is shared by $N_i = 112$ basis functions.

For the problem under consideration, the most important property of the basis functions is their hierarchical structure. The continuity of the normal component of the current flowing across the edge of the patch is ensured by the linear functions $(1 - \xi)$ and $(1 + \xi)$ in the first line of (12). At the same time, the higher order terms in the second line of (12) are zero at $\xi = \pm 1$ and do not contribute to the continuity of the current. Therefore, the order of the expansion can be different on neighboring patches. This feature is very useful when the object penetrates the interface between media, since the order of the expansion on each patch can be selected adaptively, depending on the wavelength in the medium in which the patch is located. Although the geometrical area of the patches might be the same, we can properly handle the different wavelengths in different media, avoiding unnecessary unknowns and keeping the mesh uniform. The independent selection of the expansion order in the u and v directions provides additional flexibility to the discretization technique. Consequently, even patches that are far from square can be treated in an efficient manner without introducing unnecessary unknowns.

III. Numerical Results

In this section, we present numerical examples for validation of the developed higher order discretization scheme and compare it with accelerated low-order methods, such as FMM and MLFMM. The first example validates the higher order convergence by comparing with analytical results for a PEC sphere in free space. For the next two examples (a small half-buried PEC sphere and a buried UXO), reference results are available in the literature, and we use them to validate our model for layered media. Favorable properties of the higher order solution are illustrated and compared with low-order methods. In the last example, new results for a medium sized object half-buried in the soil are presented to demonstrate the efficiency of the higher order MoM.

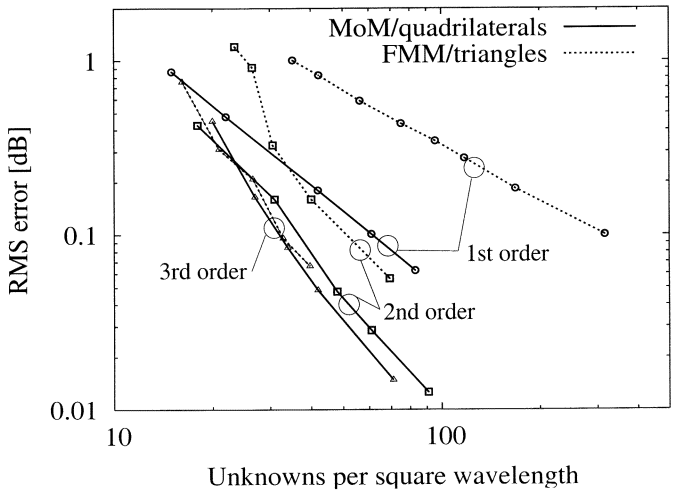

Fig. 1. RMS error for the bistatic RCS of a 9λ diameter sphere. The error for first- (circles), second- (squares), and third-order (triangles) basis functions are shown. The higher order MoM (solid lines) is compared to the MLFMM [30] using triangular patches and interpolatory basis functions (dashed lines).

A. PEC Sphere in Free Space

A PEC sphere in free space is an excellent object for validation purposes, since an exact solution exists. The exact solution used here was obtained by a Mie series [29]. We choose to measure the accuracy of a given solution through the root-mean-square (RMS) error of the bistatic radar cross section (RCS) defined as

$$\text{RMS} = \sqrt{\frac{1}{N_s}\sum_{i=1}^{N_s} |\sigma_{\text{ex}} - \sigma_{\text{MoM}}|^2} \tag{14}$$

where N_s is the number of sampling points (look angles), and σ_{MoM} and σ_{ex} are the MoM and the exact RCS measured in decibels, respectively. The RMS error is defined as in [30] to facilitate a comparison. Fig. 1 displays the RMS error as a function of the density of unknowns per λ^2 for first-, second-, and third-order basis functions. The object is a 9λ-diameter PEC sphere illuminated by a plane wave, and the curves were obtained by sampling the bistatic RCS at 360 angles in the E-plane. The solid lines show the error of the MoM using hierarchical basis functions and quadrilateral patches. It is observed that the error decays significantly faster when second-order basis functions are used instead of first-order basis functions. Thus, the desired higher order convergence has been achieved, and a large reduction in the number of unknowns is possible by using the higher order basis functions. The third-order basis functions provide even higher accuracy although the slope of the curve seems to be almost the same as for the second-order curve. This probably indicates that the RMS error for the third-order basis functions is dominated by geometrical modeling errors. Specifically, only second-order quadrilaterals were used to model the sphere, and the third-order results were obtained using quite coarse meshes. Modeling of the sphere with higher order quadrilaterals would

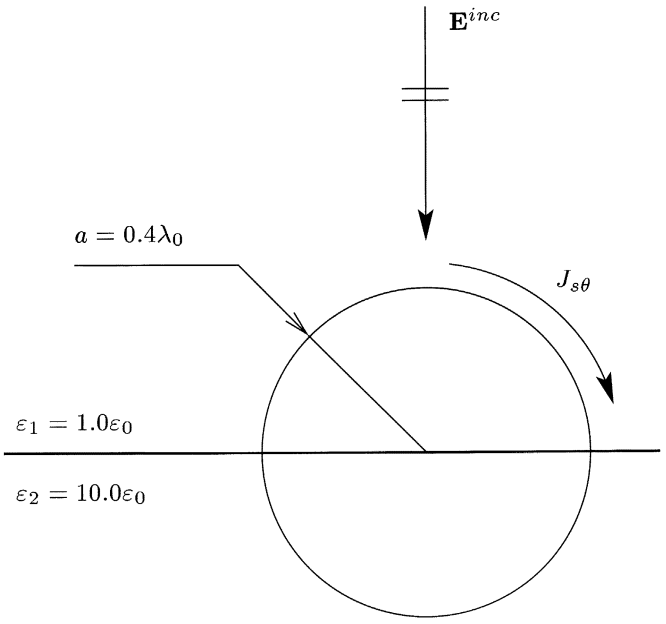

Fig. 2. Half-buried PEC sphere illuminated by a plane wave.

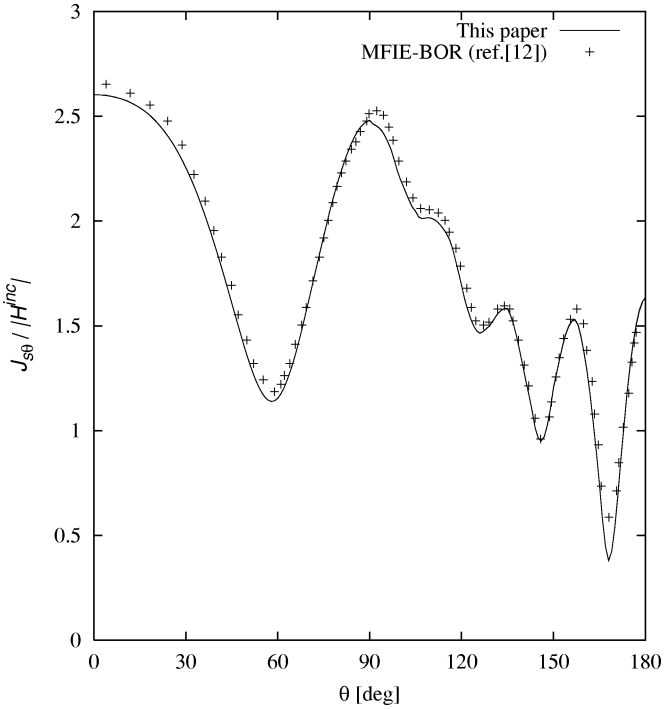

Fig. 3. Normalized magnitude of the surface current density $J_{s\theta}$ on the half-buried PEC sphere.

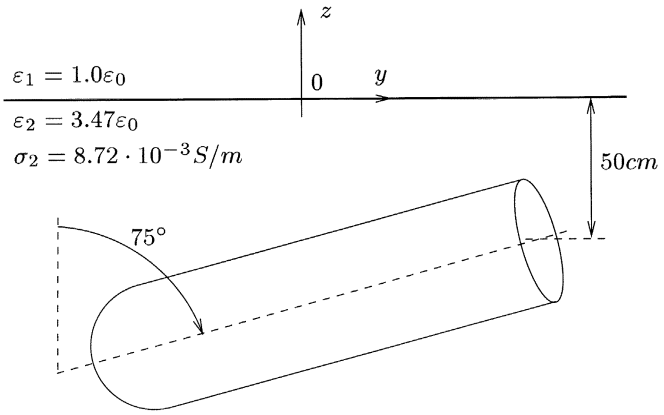

Fig. 4. UXO model. Buried cylinder with spherical cap.

of course increase the accuracy of the solution. However, the conclusions on the improved accuracy of the higher order MoM would remain the same.

Fig. 1 also displays the higher order MLFMM result reproduced from [30]. These results were obtained with triangular patches and higher order interpolatory basis functions that do not allow the flexible selection of polynomial degree suggested in this paper. Generally, the hierarchical MoM presented here is much more accurate than the interpolatory MLFMM of [30]. Particularly, the first-order curves, corresponding to rooftop and RWG basis functions, differ significantly. As an example, the basis function density required to achieve a 0.1-dB error is $70/\lambda^2$ for MoM using rooftops and more than $300/\lambda^2$ for MLFMM using RWGs. The third-order curves are quite close for MoM and MLFMM. However, the data for memory consumption given in [30] reveal that the parameters used in the MLFMM were chosen differently for the first-, second-, and third-order results and that the third-order result needed almost the same memory as a pure MoM solution. This explains why the difference between MoM and MLFMM decreases as the polynomial order increases.

B. Half-Buried PEC Sphere

A PEC sphere of radius $a = 0.4\lambda_0$ is half-buried in a lossless medium with permittivity $\varepsilon_2 = 10.0\varepsilon_0$. The upper medium is free space. The sphere is illuminated by a plane wave normally incident from above, as shown in Fig. 2. Due to the fact that the radius a is small compared to the wavelength, the surface of the sphere is discretized using $0.05\lambda_0 \times 0.05\lambda_0$ patches. Consequently, the first-order current expansion is sufficiently accurate in this case. The reference data for this problem is available from [12], where it was solved by the MFIE–BOR method [12]. Fig. 3 shows the normalized surface current density $J_{s\theta}$ along the meridian of the sphere in the plane of the incident electric field vector $\mathbf{E}^{\text{inc}}$. It is observed that the results of the present technique are in good agreement with the reference. In the next example, we present a case that cannot be treated by the MFIE–BOR method.

C. Buried UXO

We consider a model of an UXO consisting of a cylinder with a spherical cap, as shown in Fig. 4. The length of this scattering object is 153 cm, the diameter is 40.6 cm, and its axis lies in the yz plane and is tilted 75° with respect to the vertical axis. The UXO is completely buried in Yuma soil with 5% water content, for which the constitutive parameters are estimated from [31, Fig. 2]. The permittivity ε_2 is equal to $3.47\varepsilon_0$, and the conductivity is $\sigma_2 = 8.72 \cdot 10^{-3}$ S/m. A plane wave with frequency 500 MHz illuminates the UXO from the direction specified by $\theta^{\text{inc}} = 60°$ and $\phi^{\text{inc}} = 0°$. The bistatic RCS in a cut specified by $\theta^{\text{scat}} = 50°$ and $-180° \leq \phi^{\text{scat}} \leq 180°$ are shown in Fig. 5. The maximum order of the basis functions is $M^{\xi} = 2$, and the total number of unknowns is $N = 704$, corresponding

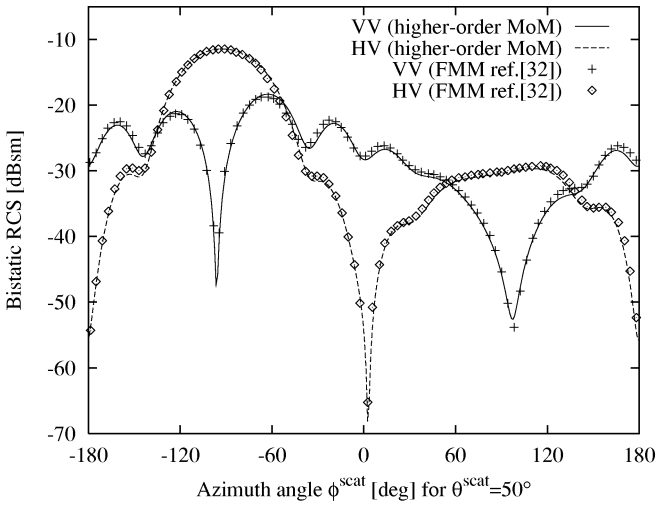

Fig. 5. Bistatic RCS of the UXO buried in Yuma soil with 5% water content.

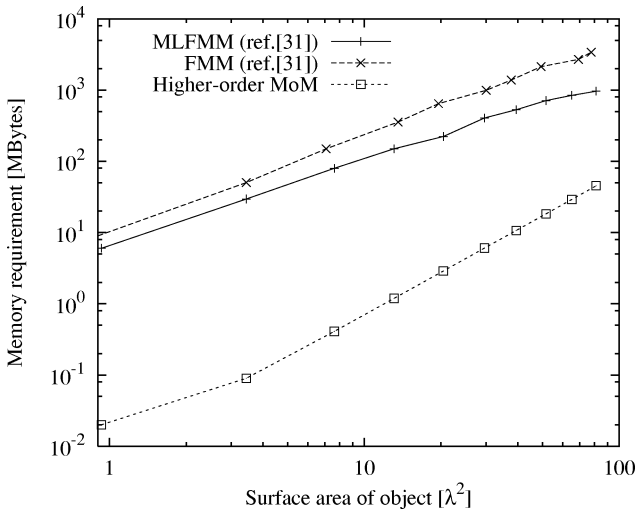

Fig. 6. Required computer memory for the bistatic RCS calculation for the buried UXO. The higher order MoM is compared with FMM and MLFMM [31].

to 34 basis functions per square wavelength in average. Fig. 5 also shows an FMM result from [32]. The agreement of the higher order MoM presented here and the FMM of [32] is excellent. However, according to [32], the FMM solution requires $N = 7167$ RWG basis functions, which is approximately five times more than required by the higher order MoM method of this paper.

This example illustrates one advantage of the higher order method. Although the computational complexity of MoM $(O(N^2))$ is higher than for FMM $(O(N^{1.5}))$ and MLFMM $(O(N \log N))$, the large reduction in the number of unknowns provided by the higher order expansion yields a more efficient solution. The memory usage of an MLFMM and an FMM implementation are reported in [31]. Here, we compare the memory usage as a function of the surface area of the object (in square wavelengths), since this parameter can be directly compared for MLFMM, FMM, and the higher order MoM. In Fig. 6, the memory requirements for MLFMM and FMM, as given in [31], are compared to the memory requirement of the higher order MoM presented here. For the frequencies considered in [31], the MLFMM requires at least ten times more memory than the higher order MoM. However, the MoM curve in Fig. 6 has a higher slope than the FMM and MLFMM, thus indicating the higher computational complexity. By extrapolating the curves in Fig. 6, one finds that the MLFMM and the higher order MoM will use the same memory when the surface area is considerably larger than 1000 square wavelengths, which corresponds to a memory requirement of much more than 10 GB. Thus, for many practical problems that can be solved on even quite powerful workstations, the higher order MoM requires less memory than the MLFMM.

The higher order method is not only competitive in terms of memory requirement but also in terms of CPU time. To show this, we employ rooftops $(M^\xi = 1)$ and higher order basis functions of orders $M^\xi = 2, 3, 4, 5$ to discretize the UXO considered above. All parameters are the same as above, except that the frequency is 1.0 GHz, the permittivity is $\varepsilon_2 = 6.4\varepsilon_0$, and the conductivity is $\sigma_2 = 3.06 \cdot 10^{-2}$ S/m corresponding to 10% water content Yuma soil. The matrix fill time and the required

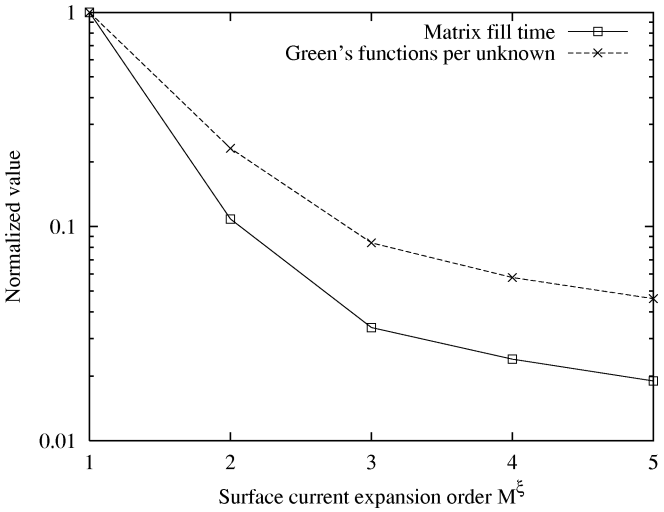

Fig. 7. Matrix fill time (solid line) and the number of multilayer Green's function evaluations per unknown (dashed line) normalized to the corresponding values for the first-order $(M^\xi = 1)$ solution as a function of the current expansion order for the UXO buried in Yuma soil with 10% water content.

number of Green's function evaluations per unknown are presented in Fig. 7 for increasing expansion order. These quantities were measured on a personal computer and normalized to the corresponding values for the first-order (rooftop) solution. In all cases, the solutions converged to a relative residual error of 10^{-4} in less than 30 iterations with the generalized minimal residual (GMRES) algorithm [33], indicating a low matrix condition number that does not increase for increasing expansion order. It can be concluded from Fig. 7 that a considerable saving in the matrix fill time is achieved by increasing the expansion order. This is not only due to the decreasing number of unknowns but also due to the fact that each integration point in the higher order MoM is shared by a large number of basis function (as discussed in Section II-E). This is illustrated by the curve showing the number of Green's function evaluations per unknown, which decreases rapidly as the expansion order increases.

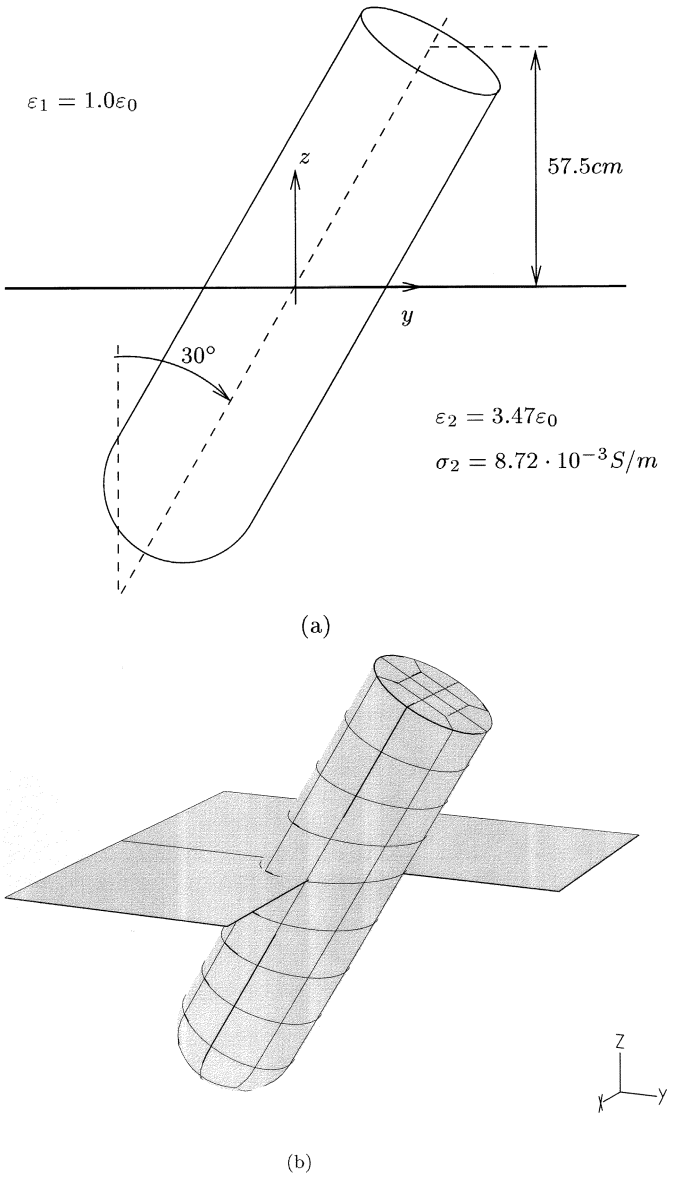

Fig. 8. Model of the UXO half-buried in Yuma soil with 5% water content. (a) Geometry of the problem. (b) Mesh of the UXO.

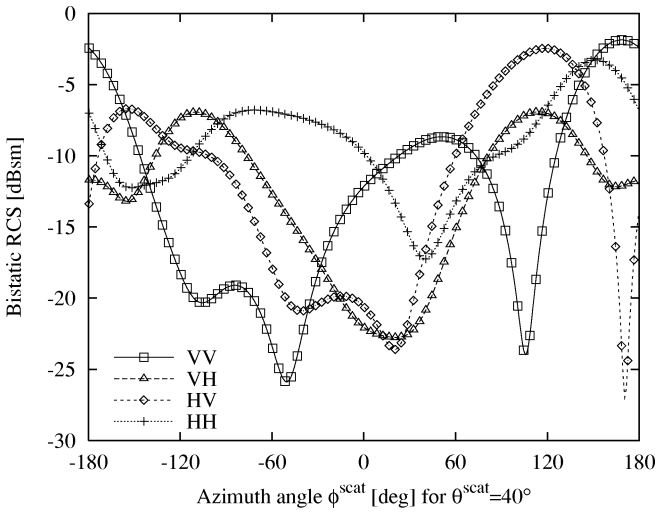

Fig. 9. Bistatic RCS of the UXO half-buried in Yuma soil with 5% water content.

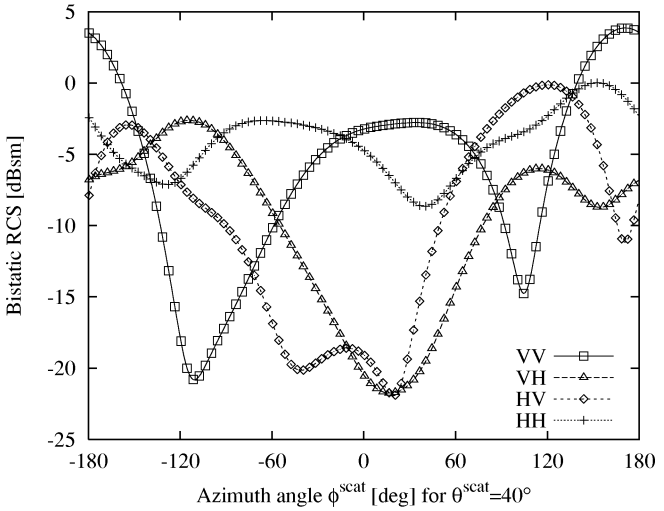

Fig. 10. Bistatic RCS of the UXO half-buried in Yuma soil with 20% water content.

D. Half-Buried UXO

The flexible selection of polynomial expansion order in the higher order hierarchical MoM makes it even more efficient if an object spans more than one medium. This is illustrated in the next example shown in Fig. 8 in which the object penetrates the interface between air and Yuma soil with 5% water content, as in the previous example. The UXO's axis is in the yz plane and is tilted 30° with respect to the vertical direction. The plane wave illuminates the object at 500 MHz from the direction specified by $\theta^{\text{inc}} = 60°$ and $\phi^{\text{inc}} = 0°$. The bistatic RCS in the cut $\theta^{\text{scat}} = 40°$ and $-180° \leq \phi^{\text{scat}} \leq 180°$ computed with 651 unknowns is presented in Fig. 9. Compared to the previous case, a further reduction in the number of unknowns is achieved due to the adaptive selection of the expansion order on each patch depending on the wavelength in the surrounding medium. However, a low-order FMM or MLFMM solution using a uniform mesh would still use 7167 unknowns as in the previous example.

Because the contrast in relative permittivities between the media is small, the reduction in number of unknowns seems insignificant in the above example. However, as the permittivity of the soil increases, the difference in the current expansion orders becomes substantial. For instance, for the same UXO as in Fig. 8, but half-buried in Yuma soil with 20% water content, which corresponds to $\varepsilon_2 = 21.45\varepsilon_0$, and conductivity $\sigma_2 = 5.34 \cdot 10^{-2}$ S/m, we use a maximum fifth-order expansion in the soil, and a maximum second-order expansion in the air. Fig. 10 shows the bistatic RCS for the same angle parameters as in the last case with the total number of unknowns $N = 2048$. The surface area of the UXO is 2.1 m^2, which is equivalent to $68.7\lambda^2$, where λ is the local wavelength. The surface area of the UXO's part located in the air is only $2.7\lambda_1^2$, and the surface area of the buried part is $66.0\lambda_2^2$. For this example, the MLFMM utilizing a uniform mesh would have to base the mesh on the shortest wavelength, which would result in the total surface area $124\lambda_2^2$ and, consequently, a huge number of unknowns.

IV. Conclusion

A higher order MoM scheme has been presented for solving surface integral equations for PEC objects in layered media. The discretization scheme employs higher order curved patches for the geometry modeling along with higher order hierarchical basis functions based on orthogonal Legendre polynomials. The hierarchical basis provides great flexibility and yields a significant reduction of the number of unknowns. Thus, when an object spans more than one media, the overdiscretization often required by lower order methods can be avoided by an adaptive selection of the expansion order on each patch. For simulation in a wide frequency band, the higher order MoM allows the mesh to be kept unchanged by varying the expansion order of the surface current density with frequency. In addition, the presented numerical examples show that the higher order MoM requires much less memory than low-order FMM or MLFMM even for fairly large problems and hence for many practical cases.

References

[1] S. M. Rao, D. R. Wilton, and A. W. Glisson, "Electromagnetic scattering by surfaces of arbitrary shape," *IEEE Trans. Antennas Propagat.*, vol. AP-30, pp. 409–418, May 1982.

[2] A. W. Glisson and D. R. Wilton, "Simple and efficient numerical methods for problems of electromagnetic radiation and scattering from surfaces," *IEEE Trans. Antennas Propagat.*, vol. AP-28, pp. 593–603, Sept. 1980.

[3] J. R. Mosig and F. E. Gardiol, "General integral equation formulation for microstrip antennas and scatterers," *Proc. Inst. Elect. Eng. H*, vol. 132, no. 7, pp. 424–432, Dec. 1985.

[4] K. A. Michalski and D. Zheng, "Electromagnetic scattering and radiation by surfaces of arbitrary shape in layered media. Part I: Theory," *IEEE Trans. Antennas Propagat.*, vol. 38, pp. 335–344, Mar. 1990.

[5] J. Chen, A. A. Kishk, and A. W. Glisson, "Application of a new MPIE formulation to the analysis of a dielectric resonator embedded in a multilayered medium coupled to a microstrip circuit," *IEEE Trans. Microwave Theory Tech.*, vol. 49, pp. 263–279, Feb. 2001.

[6] F. Ling, J. Liu, and J.-M. Jin, "Efficient electromagnetic modeling of three-dimensional multilayer microstrip antennas and circuits," *IEEE Trans. Microwave Theory Tech.*, vol. 50, pp. 1628–1635, June 2002.

[7] B. D. Popović and D. Ž. Djurdjević, "Entire-domain analysis of thin-wire antennas near or in lossy ground," *Proc. Inst. Elect. Eng., Microwave Antennas Propagat.*, vol. 142, no. 3, pp. 213–219, June 1995.

[8] W. Cai, T. Yu, H. Wang, and Y. Yu, "High-order mixed RWG basis functions for electromagnetic applications," *IEEE Trans. Microwave Theory Tech.*, vol. 49, pp. 1295–1303, July 2001.

[9] J. C. Nedelec, "Mixed finite elements in R^3," *Numer. Math.*, vol. 35, no. 3, pp. 315–341, 1980.

[10] E. Jørgensen, J. L. Volakis, P. Meincke, and O. Breinbjerg, "Higher-order hierarchical Legendre basis functions for iterative integral equation solvers with curvilinear surface modeling," *Proc. IEEE Antennas Propagation Society Int. Symp.*, vol. 4, pp. 618–621, June 2002.

[11] B. M. Kolundžija and B. D. Popović, "Entire-domain galerkin method for analysis of metallic antennas and scatterers," *Proc. Inst. Elect. Eng. H*, vol. 140, no. 1, pp. 1–10, Feb. 1993.

[12] A. A. K. Mohsen and A. K. Abdelmageed, "Magnetic field integral equation for electromagnetic scattering by conducting bodies of revolution in layered media," *Progr. Electromagn. Res.*, vol. 24, pp. 19–37, 1999.

[13] A. J. Poggio and E. K. Miller, "Integral equation solutions of three-dimensional scattering problems," in *Computer Techniques for Electromagnetics*, R. Mittra, Ed. New York: Pergamon, 1973, pp. 159–264.

[14] K. A. Michalski, "The mixed-potential electric field integral equation for objects in layered media," *Arch. Elekt. Übertragung.*, vol. 39, pp. 317–322, Sept.–Oct. 1985.

[15] K. A. Michalski and J. R. Mosig, "Multilayered media Green's functions in integral equation formulations," *IEEE Trans. Antennas Propagat.*, vol. 45, pp. 508–519, Mar. 1997.

[16] K. A. Michalski, "On the efficient evaluation of integrals arising in the Sommerfeld halfspace problem," in *Proc. Inst. Elec. Eng. H*, vol. 132, Aug. 1985, pp. 312–318.

[17] Y. L. Chow, J. J. Yang, D. G. Fang, and G. E. Howard, "A closed-form spatial Green's function for the thick microstrip substrate," *IEEE Trans. Microwave Theory Tech.*, vol. 39, pp. 588–592, Mar. 1991.

[18] J. J. Yang, Y. L. Chow, and D. G. Fang, "Discrete complex images of a three-dimensional dipole above and within a lossy ground," *Proc. Inst. Elect. Eng. H*, vol. 138, no. 4, pp. 319–326, Aug. 1991.

[19] N. Hojjat, S. Safavi-Naeini, and Y. L. Chow, "Numerical computation of complex image Green's functions for multilayer dielectric media: Near-field zone and the interface region," *Proc. Inst. Elect. Eng.—Microwave Antennas Propagat.*, vol. 145, no. 6, pp. 449–454, Dec. 1998.

[20] M. I. Aksun and R. Mittra, "Derivation of closed-form Green's functions for a general microstrip geometry," *IEEE Trans. Microwave Theory Tech.*, vol. 40, pp. 2055–2062, Nov. 1992.

[21] G. Dural and M. I. Aksun, "Closed-form Green's functions for general sources and stratified media," *IEEE Trans. Microwave Theory Tech.*, vol. 43, pp. 1545–1552, July 1995.

[22] M. I. Aksun, "A robust approach for the derivation of closed-form Green's functions," *IEEE Trans. Microwave Theory Tech.*, vol. 44, pp. 651–658, May 1996.

[23] Y. Hua and T. K. Sarkar, "Generalized pencil-of-function method for extracting poles of an EM system from its transient response," *IEEE Trans. Antennas Propagat.*, vol. 37, pp. 229–234, Feb. 1989.

[24] N. Kinayman and M. I. Aksun, "Efficient use of closed-form Green's functions for the analysis of planar geometries with vertical connections," *IEEE Trans. Microwave Theory Tech.*, vol. 45, pp. 593–603, May 1997.

[25] Y. Liu, L.-W. Li, T.-S. Yeo, and M.-S. Leong, "Application of DCIM to MPIE-MoM analysis of 3D PEC objects in multilayered media," *IEEE Trans. Antennas Propagat.*, vol. 50, pp. 157–162, Feb. 2002.

[26] D. R. Wilton, S. M. Rao, A. W. Glisson, D. H. Schaubert, O. M. Al-Bundak, and C. M. Butler, "Potential integrals for uniform and linear source distributions on polygonal and polyhedral domains," *IEEE Trans. Antennas and Propagation*, vol. AP-32, pp. 276–281, Mar. 1984.

[27] K. Sertel and J. L. Volakis, "Method of moments solution of volume integral equations using parametric geometry," *Radio Sci.*, vol. 37, no. 1, pp. 1–7, Jan.–Feb. 2002.

[28] M. G. Duffy, "Quadrature over a pyramid or cube of integrands with a singularity at a vertex," *SIAM J. Numer. Anal.*, vol. 19, no. 6, pp. 1260–1262, Dec. 1982.

[29] W. Wiscombe, "Improved Mie scattering algorithms," *Appl. Opt.*, vol. 19, pp. 1505–1509, 1980.

[30] K. C. Donepudi, J.-M. Jin, S. Velamparambil, J. Song, and W. C. Chew, "A higher order parallelized multilevel fast multipole algorithm for 3-D scattering," *IEEE Trans. Antennas Propagat.*, vol. 49, pp. 1069–1078, July 2001.

[31] N. Geng, A. Sullivan, and L. Carin, "Multilevel fast-multipole algorithm for scattering from conducting targets above or embedded in a lossy half space," *IEEE Trans. Geosci. Remote Sensing*, vol. 38, pp. 1561–1573, July 2000.

[32] ——, "Fast multipole method for scattering from an arbitrary PEC target above or buried in a lossy half space," *IEEE Trans. Antennas Propagat.*, vol. 49, pp. 740–748, May 2001.

[33] Y. Saad, *Iterative Methods for Sparse Linear Systems*, 1st ed. Boston, MA: PWS, 1996. See http://www-users.cs.umn.edu/~saad/books.html.

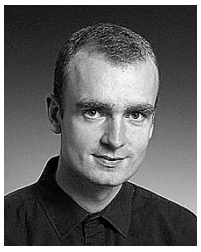

Erik Jørgensen (S'99–M'03) was born in Denmark in 1974. He received the M.S. and Ph.D. degrees in electrical engineering from the Technical University of Denmark, Lyngby, in 2000 and 2003, respectively.

In the fall of 1998, he spent five months at the Department of Information Engineering, University of Siena, Siena, Italy. In the fall of 2001, he was a Visiting Scholar with the Radiation Laboratory, University of Michigan, Ann Arbor. In 2003, he joined the Danish company TICRA, Copenhagen, Denmark. His research interests include computational electromagnetics and high-frequency techniques.

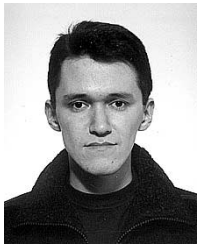

Oleksiy S. Kim received the M.S. and the Ph.D. degrees from the National Technical University of Ukraine, Kiev, in 1996 and 2000, respectively, both in electrical engineering.

During his Ph.D. studies, his work has been primarily concerned with synthesis and optimization of reflector antennas and feed horns, analysis of waveguide structures, and discontinuities. In 2000, he joined the Antenna and Electromagnetics Group, Technical University of Denmark (DTU), Lyngby. He is currently an Associate Professor at Ørsted-DTU. His research interests include computational electromagnetics, scattering, microstrip antenna design, and ground-penetrating radars.

Peter Meincke (S'93–M'96) was born in Roskilde, Denmark, on November 25, 1969. He received the M.S.E.E. and Ph.D. degrees from the Technical University of Denmark (DTU), Lyngby, in 1993 and 1996.

In the spring and summer of 1995, he was a Visiting Research Scientist with the Electromagnetics Directorate of Rome Laboratory, Hanscom Air Force Base, MA. In 1997, he was with a Danish cellular phone company, working on theoretical aspects of radio-wave propagation. In the spring and summer of 1998, he was visiting the Center for Electromagnetics Research, Northeastern University, Boston, MA, while holding a Postdoctoral position from DTU. In 1999, he became a staff member of the Department of Electromagnetic Systems, DTU. He is currently an Associate Professor with Ørsted-DTU. His current teaching and research interests include electromagnetic theory, inverse problems, high-frequency and time-domain scattering, antenna theory, and ground-penetrating radars.

Dr. Meincke won the first prize award in the 1996 IEEE Antennas and Propagation Society Student Paper Contest in Baltimore, MD, for his paper on uniform physical theory of diffraction equivalent edge currents. Also, he received the 2000 RWP King Paper Award for his paper "Time-Domain Version of the Physical Theory of Diffraction" published in the February 1999 issue of the IEEE TRANSACTIONS ON ANTENNAS AND PROPAGATION.

Olav Breinbjerg (M'87) was born in Silkeborg, Denmark on July 16, 1961. He received the M.S.E.E. and Ph.D. degrees from the Technical University of Denmark (DTU), Lyngby, in 1987 and 1992, respectively.

Since 1991, he has been on the faculty of Ørsted-DTU, Electromagnetic Systems, DTU, where he is currently an Associate Professor and Head of the Antenna and Electromagnetics Group comprising also the DTU-ESA Spherical Near-Field Antenna Test Facility. He was a Visiting Research Scientist at the Rome Laboratory, Hanscom Air Force Base, MA in the fall of 1988 and a Fulbright Scholar at the University of Texas, Austin, in the spring of 1995. His research interests include electromagnetic field theory, asymptotic and computational electromagnetics, antennas, and scattering.